

# Repetitively pulsed regime of Nd:glass large-aperture laser amplifiers

A.A. Kuzmin, E.A. Khazanov, A.A. Shaykin

**Abstract.** A repetitively pulsed operation regime of neodymium glass rod laser amplifiers with apertures of 4.5, 6, 8.5, and 10 cm is analysed using experimental data. The limits of an increase in the pulse repetition rates are determined. Universal dependences are obtained, which help finding a compromise between increasing the repetition rate and enhancing the gain for each particular case. In particular, it is shown that an amplifier 4.5-cm in diameter exhibits a five-fold safety factor with respect to a thermo-mechanical breakdown at a repetition rate of 1 pulse  $\text{min}^{-1}$  and stored energy of above 100 J. A strong thermally induced birefringence in two such amplifiers is experimentally reduced to a ‘cold’ level by employing a 90° optical rotator.

**Keywords:** neodymium glass amplifiers, repetitively pulsed operation regime, thermally induced polarisation and phase distortions of radiation, compensation of depolarisation.

## 1. Introduction

Neodymium glass laser amplifiers are widely used in numerous laser devices of a petawatt power level. All existing and designed petawatt lasers are divided into the three types: with a neodymium glass active medium [1], sapphire (corundum with titanium) medium [2], and lasers with parametric amplification on KDP and DKDP crystals [3]. In the second and third types of lasers, radiation of a neodymium glass laser transformed into second harmonic is used for pumping either a sapphire crystal or a parametric amplifier of chirped pulses, respectively.

The main advantage of neodymium glass is a possibility to fabricate large-aperture active elements, capable of storing a large amount of energy and operating at a relatively low intensity of laser radiation below an optical breakdown threshold. However, a relatively low thermal conductivity of neodymium glass noticeably limits the repetition rate of laser pulses. A principal limitation is a breakdown of an active element if admissible elastic stresses are exceeded. If the time lapse between pump pulses is shorter than a characteristic cooling time for the active element, then a gradual accumulation of heat inside the active medium would noticeably change polarisation and phase of radiation due to a photoelastic effect.

A.A. Kuzmin, E.A. Khazanov, A.A. Shaykin Institute of Applied Physics, Russian Academy of Sciences, ul. Ul’yanova 46, 603950 Nizhnii Novgorod, Russia; e-mail: alexeyhsgap@yandex.ru, khazanov@appl.sci-nnov.ru, shaykin@appl.sci-nnov.ru

Received 19 October 2011.

Kvantovaya Elektronika 42 (4) 283–291 (2012)

Translated by N.A. Raspopov

Thermally induced birefringence was thoroughly studied theoretically and experimentally in [4–13]. Nevertheless, in publications devoted to operation of lasers with a pulse energy  $W \geq 100$  J, the problem of thermally induced birefringence was not actually discussed. For example, less than 3% of all polarisation losses on the ‘Omega’ laser complex reported in [14] are discussed. Such a situation is typical for a single pulse regime where heat is not accumulated from shot to shot, and heating the active element by single pulses is sufficiently uniform and induces no noticeable elastic stresses.

In [15], we studied a repetitively pulsed regime of high-power large-aperture laser amplifiers with neodymium glass active media with diameters of 6, 8.5, and 10 cm under repetitively pulsed pumping with the period of 3 min. Such amplifiers constitute a pump system of a parametrical laser setup PEARL (PEtawatt pARAMetrical Laser) with an output power of 0.56 PW [3]. The time of rod cooling-down  $\tau$  is proportional to the square radius of the rod. Just amplifiers with a greater diameter undergo higher thermal load because, under intense cooling of the rod generatrix, the time is  $\tau = R^2/(5.76\kappa)$ , where  $R$  is the rod radius and  $\kappa$  is thermal diffusivity factor. By the results of depolarisation measurements the increase in rod temperature caused by a single pump pulse was calculated in [15] using a relationship between the depolarisation of radiation and distribution of temperature. From known temperature distributions arising in rods after a single pump pulse, we calculated dynamics of temperature and of thermally induced lens and then estimated thermally induced elastic stresses in the active elements. In the active element with the diameter  $D_1 = 10$  cm the thermally induced stresses were 15% (30%) of the threshold value at the repetition rate of 1 pulse per 3 (1.5) min. For increasing the pulse repetition rate one may reduce the energy of the discharge in pump flashlamps of large-aperture amplifiers (this reduces a heat load on the active element, but lowers the stored energy) or employ a new laser scheme comprising active elements of shorter diameter capable of operating at higher pulse repetition rates without destruction.

In the present work, we experimentally study thermally induced effects in an amplifier 4.5-cm in diameter in the operation regime with the pulse repetition period of 1 min. Using these measurements and results presented in [15] we thoroughly analysed thermally induced effects in the amplifiers under study at arbitrary repetition rates of pump pulses. Then, we plotted dependences, which in every particular case allow one not only to determine a maximal admissible repetition rate, but also to find a compromise between the repetition rate raise and gain increase.

Based on the results obtained, we suggest a project of a neodymium laser with the pulse energy of 340 J (the pulse duration of 20 ns) and the pulse repetition period of 1 min.

Second harmonic of the laser radiation is used for pumping a Ti:Sapphire crystal of a chirped pulse amplifier. Main load-bearing elements of the setup are neodymium glass rods with the diameter of 4.5 cm already tested at the repetition rate of 1 pulse  $\text{min}^{-1}$ . Strong thermally induced distortions of radiation are supposed to be compensated by a  $90^\circ$  polarisation rotator.

## 2. Parameters of studied rod active elements made of neodymium glass

Results of an experimental study of thermally induced radiation distortions are published in [15] for KGSS-1621 neodymium glass rods (the parameters of glass GLS-22, similar in physical properties, are given in [16]) with the diameters of 6, 8.5, and 10 cm employed in amplifiers with the pump pulse repetition period of 3 min. In the present work, we present results of similar investigations with a rod of the same type and the diameter of 4.5 cm at a pulse repetition period of 1 min (see Section 3). Main characteristics of the amplifiers under study are given in Table 1. The active elements with diameters of 6, 8.5, and 10 cm were pumped by eight IFP-8000 flashlamps. A maximal pump energy  $W_p$  was 36.5 kJ (two capacitors 200  $\mu\text{F}$  each could be charged up to 13.5 kV [17]). The active element with a diameter of 4.5 cm was pumped by six IFP-5000-2 flashlamps. A maximal pump energy in this case was 23.8 kJ (three capacitors 324  $\mu\text{F}$  each charged up to 7 kV).

In all the experiments, we used quantrons with mirror reflectors. Figure 1 shows the amplifier cross sections. Each section of the reflector has the ‘Winston’ shape [18]. Such a reflector efficiently transfers the energy from the lamp surface to the surface of an active element. Cylindrical surfaces of the active element (with the diameter  $D_1$ ), water around the element

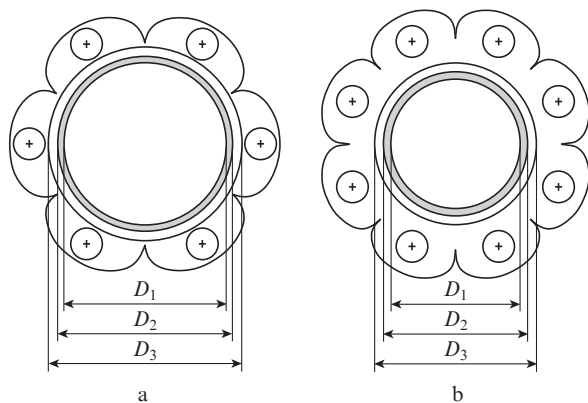


**Figure 1.** Cross sections of amplifiers comprising six pump flashlamps (the diameter of active element is 4.5 cm) (a) and eight pump flashlamps (the diameter of active element is 6, 8.5, or 10 cm) (b).

**Table 1.** Characteristics of investigated laser amplifiers.

$D_1/$ cm	$L/$ cm	$D_2/$ cm	$D_3/$ cm	$[\text{Nd}^{3+}]/$ $10^{20} \text{ cm}^{-3}$	$\alpha/$ $10^{-3} \text{ cm}^2 \text{ s}^{-1}$	Flashlamp type	$N_1$	$N_{st}$	$C/$ $\mu\text{F}$	$U_{max}/$ kV	$N_1/N_{st}$	$W_p/$ kJ	$\langle G_0 \rangle$	$W_{st}/$ J	$W_1/$ J	$W_2/$ kJ
4.5	25	4.8	5.4	0.86	2.8	IFP-5000-2	6 (Fig. 1a)	3	324	7	2	23.8	7.4	112	113.2	8.6
6	25	9.5	10.0	0.56	2.0	IFP-8000	8 (Fig. 1b)	2	200	13.5	4	36.5	6.5	184	191.7	19.0
8.5	25	10.8	11.4	0.29	2.5	IFP-8000	8 (Fig. 1b)	2	200	13.5	4	36.5	3.8	264	284.8	22.3
10	25	10.8	11.4	0.33	2.5	IFP-8000	8 (Fig. 1b)	2	200	13.5	4	36.5	2.8	282	287.9	15.9

Note:  $L$  is the length of active element,  $N_1$  is the number of flashlamps,  $N_{st}$  is the number of capacitive storages,  $C$  is the capacity of a capacitive storage,  $N_1/N_{st}$  is the number of flashlamps per capacitive storage (connected in series).

( $D_2$ ), and a glass bulb ( $D_3$ ) affect focusing of radiation onto the active element, and hence, influence the amplifier efficiency and gain cross-section distribution in the active element [17]. The active elements were cooled by flowing water with the entry temperature stabilised within an accuracy of  $\pm 0.1$  K. In Table 1, for the amplifiers studied, the small-signal gain averaged over the aperture of an active element ( $\langle G_0 \rangle$ ) is given along with the stored energy  $W_{st}$  at a maximal pump energy  $W_p$ . In calculating  $W_{st}$  we assumed the saturated energy density for neodymium glass  $3.5 \text{ J cm}^{-2}$  and made allowance for non-uniform gain cross-section distribution in the active elements [15, 17].

In Fig. 2, the energy stored in the active elements is shown versus the pump energy. The experimental results are approximated by curves of the type  $W_{st} = W_1 \tanh(W_p/W_2)$ , where the parameters  $W_1$  and  $W_2$  for each active element are given in Table 1. Below, this formula will be used for analysing possible operation regimes of the amplifiers. Note that at low

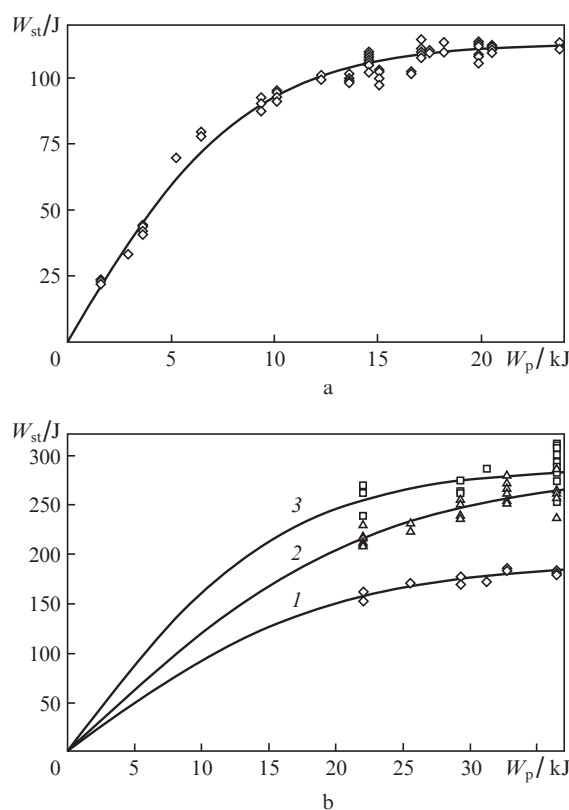


**Figure 2.** Energy stored in active elements with the diameters of 4.5 cm (a), 6 cm [b, curve (1)], 8.5 cm [b, curve (2)], 10 cm [b, curve (3)] vs. the pump energy. Dots present experimental results and solid curves are the results of interpolation.

pump energies there are no experimental points for the active elements with the apertures of 6, 8.5, and 10 cm in Fig. 2b. This is explained by specific technical ignition of flashlamps. In the amplifier with the active element diameter of 4.5 cm, two flashlamps connected in series were initiated by a current pulse from an external ignition unit. Parameters of the pulse were independent of the voltage across capacitors; hence, the pump lamps operated at a low charge as well. In all other amplifiers, four flashlamps connected in series were initiated by a pulse formed in an additional low-energy pre-ionising contour; thus, ignition of lamps only occurred at a voltage above a certain threshold value ( $\sim 10.5$  kV) [17].

### 3. Measurement of thermally induced radiation distortions in an active element with a diameter of 4.5 cm

Thermally induced distortions of radiation in the rod with a diameter of 4.5 cm were studied at the pulse repetition period of 1 min. At so high a repetition rate, the temperature of flashlamps raises in addition to active element heating. Under such conditions, a quartz bulb of the flashlamp becomes dim and heat expansion leading to high elastic stresses near places of lamp attachment to a quantron case may breakdown the lamp. Such phenomena were observed in experiments with the active element 6 cm in diameter. Air in the space of the quantron where the flashlamps reside (between a metal case and water bulb with an active element) behaves as a thermos preventing lamp cooling after shots. In the operation regime of 1 shot per 2 min (the energy of lamp discharge was 36.5 kJ), the flashlamps were broken after a series of 27 shots. In the experiments with the active element 4.5 cm in diameter in the operation regime of 1 pulse  $\text{min}^{-1}$ , the flaslamps were cooled by flowing air at room temperature in order to prevent flashlamp breakdown and dim. The active element was cooled by flowing water. The pump energy was 17.5 kJ.

Particular attention in our experiments was paid to thermally induced depolarisation of radiation. The depolarisation was measured by linearly polarised probe pulses at a repetition rate of 1 Hz. The active element was placed between crossed polarisers. The value of depolarisation was determined from the ratio of input and output laser radiation intensities.

Based on the depolarisation measurements by the method described in [13, 15] we calculated a temperature distribution in a rod after a single pump pulse (at the instant of the electric discharge termination in the flashlamps). Then, we modelled a dynamics of temperature distribution, thermally induced lens, and depolarisation over the whole pulse series. Elastic and optical characteristics of KGSS-1621 glass were chosen equal to those of GLS-22 glass from [16]. A radial temperature distribution after a single pump pulse is shown in Fig. 3a. In Fig. 3b, the corresponding distributions are shown for rods with the diameters of 6, 8.5, and 10 cm [15]. To a sufficient accuracy we may assume that the temperature is proportional to the pump energy, i.e., two values of energy  $W_{p1}$  and  $W_{p2}$  are related with corresponding temperature distributions  $\Delta T_1(r)$  and  $\Delta T_2(r)$  by the relationship  $\Delta T_1(r)/\Delta T_2(r) = W_{p1}/W_{p2}$ . The assumption is experimentally confirmed: the temperature distributions in a rod with the diameter of 4.5 cm calculated from measured thermally induced depolarisation of radiation at the pump energies of 17.5 kJ and 14.6 kJ obey the above formula.

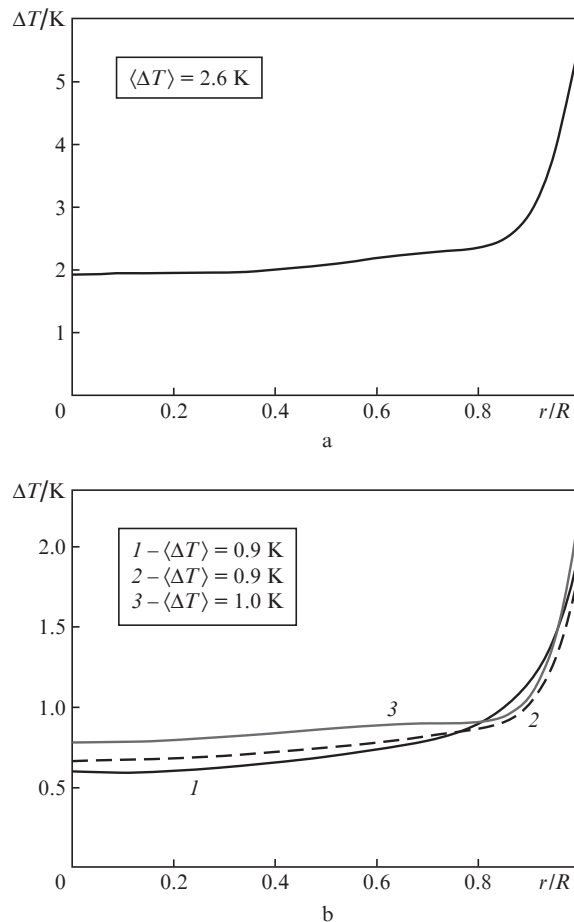


Figure 3. Temperature distributions in active elements with the diameters  $2R = 4.5$  (a), 6 [b, curve (1)], 8.5 [b, curve (2)], and 10 cm [b, curve (3)] after a single pump pulse with the energy  $W_p$  equal to 17.5 J (a) and 36.5 J (b);  $\langle \Delta T \rangle$  is the temperature of the active element averaged over its aperture and counted relative the temperature of cooling liquid.

Figure 4 shows the dynamics of the integral depolarisation factor  $\gamma$ , which is the ratio of the energy of radiation that is polarised normally to incident radiation, to the total beam energy at the exit from the active medium. The pump pulse repetition period is 1 min. The figure demonstrates both

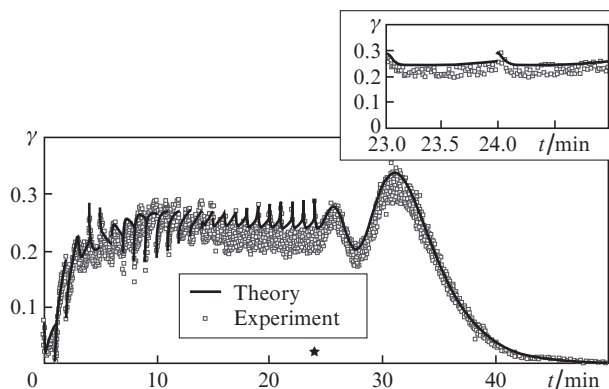
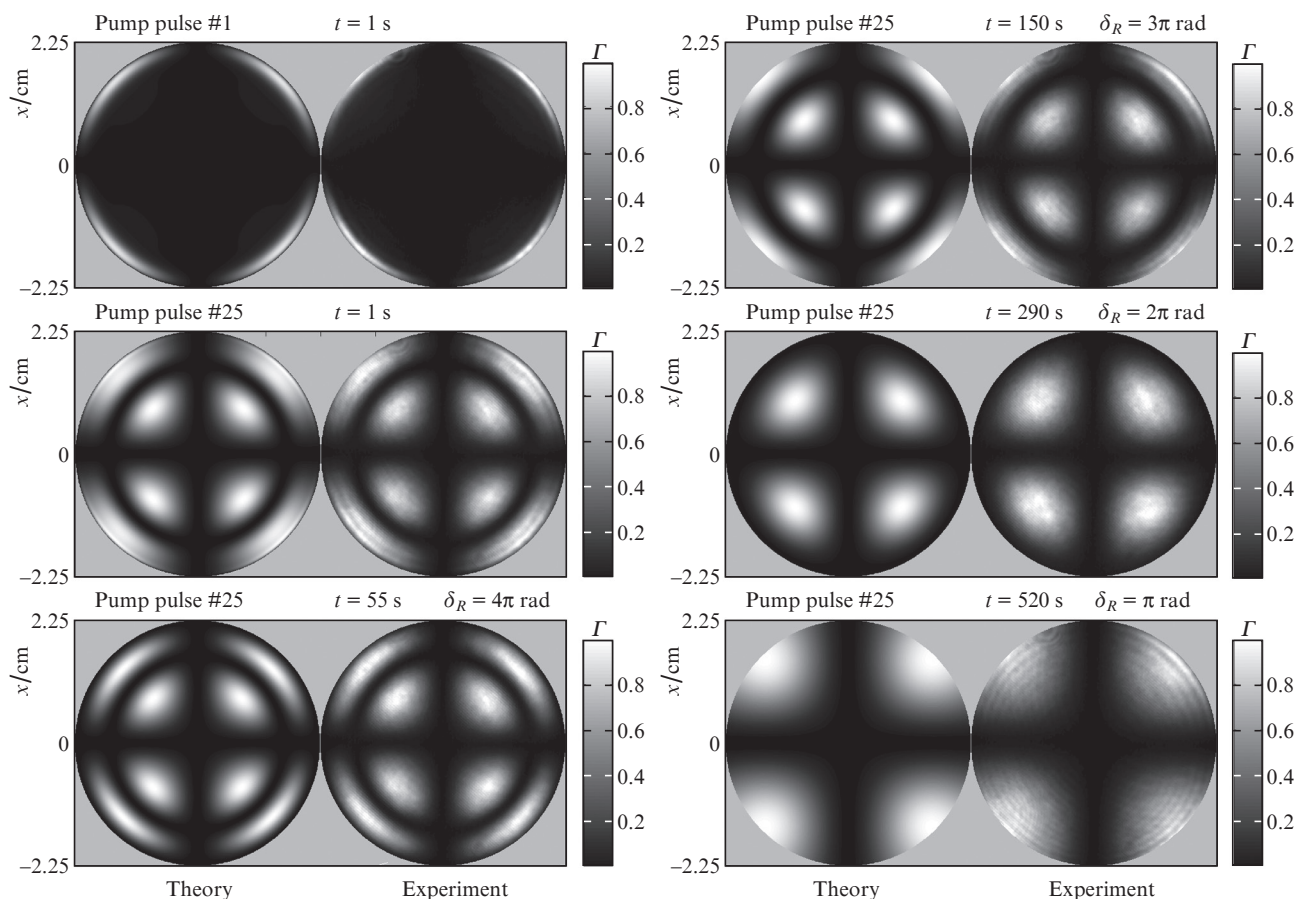


Figure 4. Dynamics of integral coefficient of depolarisation  $\gamma$  in the active element with the diameter of 4.5 cm in a series of pump pulses with the period of 1 min. An asterisk denotes the instant of the last pulse in the series.



**Figure 5.** Theoretical and experimental distributions for the depolarisation factor  $\Gamma$  in the active element with the diameter of 4.5 cm after a first pump pulse and at various instants after the last pump pulse in a series.

establishment of a stationary regime and relaxation of depolarisation after each pump pulse.

Figure 5 presents the cross-section distributions for a depolarisation factor  $\Gamma$  (the ratio of the intensity of radiation, polarised normally to an incident radiation, to the total intensity) at an exit from the active medium one second after the first pump pulse and in various time lapses after the terminating

pump pulse in the series. One can see from Figs 4 and 5 that experimental data well agree with the theoretical approach.

Figure 6 shows the calculation results of radial distributions for eigenwave phases and temperature in an active element for a stationary regime, i.e., after heat equilibrium is established. In rod geometry, due to cylindrical symmetry and glass isotropy there are two eigenwaves with radial and tan-

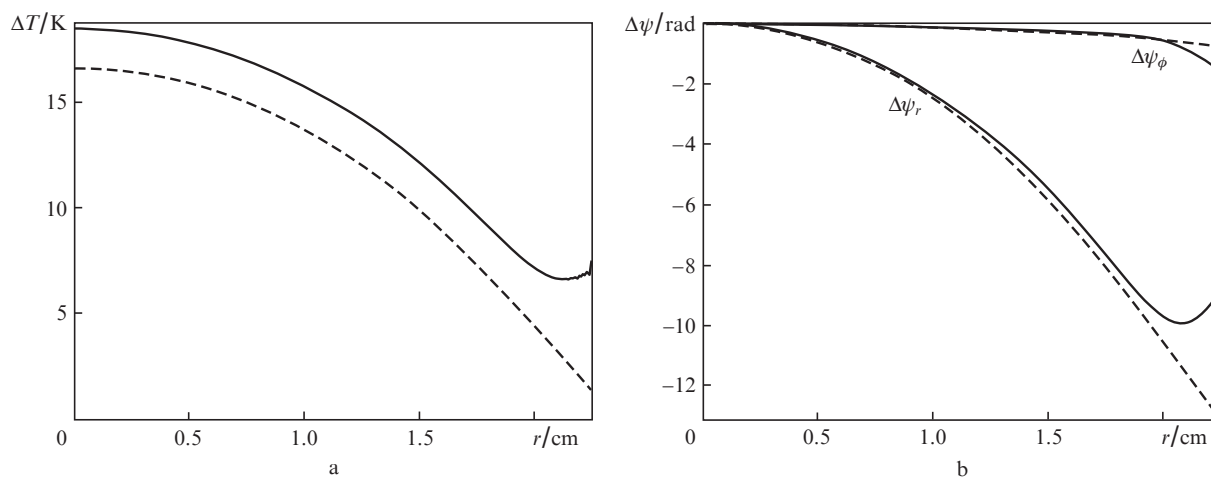


**Figure 6.** Temperature (a) and eigenwaves phase (b) distributions in the active element with the diameter of 4.5 cm in the stationary regime. Dashed curves correspond to the onset of the electric discharge in flashlamps, solid curves refer to the end of the pump pulse.

gential polarisations in the active element. We will denote the phase incursions in the active medium by  $\Delta\psi_r$  and  $\Delta\psi_\phi$ , respectively. Their difference  $\delta = \Delta\psi_\phi - \Delta\psi_r$  determines the factor of radiation depolarisation. The depolarisation factor for linearly polarised radiation at the entry into the active element is described by the formula  $\Gamma = \sin^2(2\phi)\sin^2(\delta(r, t)/2)$ . This expression is basic in our calculations of  $\Delta\psi_r$  and  $\Delta\psi_\phi$  (see [15]). We may also introduce the parameter  $\delta_R(t) = \delta(r=R, t)$ , which characterises the difference between induced phase incursions for the eigenwaves at the surface of the active element.

Analysing Fig. 6b, one can see that except for a small domain at the active element surface, the dependences  $\Delta\psi_{r,\phi}(r)$  are almost parabolic:  $\Delta\psi_{r,\phi}(r) \approx -\pi r^2/(\lambda F_{r,\phi})$ , where  $\lambda$  is the wavelength of laser radiation. The focal distances  $F_r$  and  $F_\phi$  (for the radial and tangential polarisations, respectively) of thermally induced lens are 120 and 2500 m. The focal power for the tangential polarisation  $1/F_\phi$  is so small that its accuracy is above 100%. For example, a variation of  $dn/dT$  by 3%, which was used in our calculations, may even change the sign of  $F_\phi$ .

Astigmatism ( $\Delta\psi_r \neq \Delta\psi_\phi$ ) and depolarisation of radiation may be compensated simultaneously by a 90° polarisation rotator placed between two similar active elements. In such a scheme, the resulting phase is  $\Delta\psi_2 = \Delta\psi_\phi + \Delta\psi_r$ ; it is independent of the polarisation state at the system input. The parabolic component of the lens in this case may be excluded by introducing an additional detuning to telescopes placed between the active elements.

Higher-order aberrations are noticeable at rod periphery and their influence considerably depends on the diameter and shape of the laser beam. Note that the phase distributions in Fig. 6b are obtained under the assumption that heat release in the active element due to a pump pulse has already finished at the instant of laser pulse passing. Actually, the amplified laser pulse comes at the moment of maximum population inversion and occurs yet before the pump pulse stops. A real temperature distribution at the instant of laser pulse onset resides between the distributions shown in Fig. 6a. Thus, the calculated aberrations of the thermally induced lens (see Fig. 6b) are upper estimates of real aberrations. The remarks made above have actually no effect on the calculated focal distances  $F_r$  and  $F_\phi$ .

Physical properties of KGSS-1621 glass are such that the phase incursion  $\Delta\psi_r$  of the radially polarised wave is much greater than that of the tangentially polarised wave  $\Delta\psi_\phi$  (see Fig. 6b) and we may assume  $\delta(r, t) \approx -\Delta\psi_r$ . On the other hand, during stationary laser operation we have  $\delta(r, t) \approx \delta_R(t)r^2/R^2$ . Hence, the focal distance of the thermally induced lens for the radially polarised radiation may be estimated from the formula  $F_r \approx \pi R^2/(\lambda\delta_R(t))$ , whereas phase distortions of the tangentially polarised wave may be neglected. The parameter  $\delta_R(t)$  determines the number of radial variations (circles) in a stationary distribution of the depolarisation factor; hence, it may be easily estimated experimentally. Distributions of the depolarisation factor corresponding to various values of  $\delta_R(t)$  are shown in Fig. 5.

#### 4. Analysis of thermally induced effects at various pulse repetition rates and pump energies

Active element surfaces undergo thermo-mechanical destructions to a greater degree, which is explained by numerous surface defects (microcracks, etc.) [5]. For a cylindrical active element, an elastic strength at a surface is given by the for-

mula [5]:  $\sigma = \alpha E(\langle T \rangle - T)/(1 - \nu)$ , where  $\alpha$  is the thermal linear expansion coefficient,  $E$  is the Young modulus,  $\nu$  is the Poisson ratio,  $T$  and  $\langle T \rangle$  are the surface and average rod temperatures, respectively. The utmost permissible value of  $\sigma_{lim}$  is determined by the glass heat resistance  $\delta T = (\langle T \rangle - T)_{lim}$ . We employed a phosphate KGSS-1621 glass and assumed  $\delta T = 38$  K (such heat resistance, according to [16], is specific for GLS-22 glass). The utmost elastic stresses  $\sigma_{lim}$  in this case may be estimated as 30 MPa. In what follows, considering elastic stresses we will assume the rod surface stresses.

Consider a repetitively pulsed laser operation where the pump pulses of equal energy are repeated at a repetition rate  $f$ . In such a regime, a stationary regime is established, in which the heat absorbed by active elements per single pump pulse is equal to the heat removed from their surfaces during a time lapse between neighbouring pulses. To describe the stationary state we will use the parameter  $\delta_R(t = t_p - 0)$  which characterises the difference in thermally induced phase incursions for eigenwaves at the surface of active element at the instant just before passing a next pump pulse. In what follows, if no argument is specified for  $\delta_R$  we will assume  $\delta_R(t = t_p - 0)$ .

As was already mentioned, the heat problem is linear one; hence, it is reasonable to transfer from parameter  $f$  to a more universal parameter  $P_p = fW_p$ , which characterises an average pump power. Figure 7 presents the dependence of  $\delta_R$  on  $P_p$  for the amplifiers under consideration. Note that operation of the active element under elastic stresses exceeding a breakdown threshold by 20%–30% is not reliable. This is why the range of values for  $\delta_R$  in Fig. 7 is limited to  $6\pi$  rad, which, as one can see from Fig. 8, corresponds to  $\sigma_{max} = 0.3\sigma_{lim}$ . The value of  $\gamma$  (Fig. 8) is calculated at the instant just before passing the pump pulse ( $t = t_p - 0$ ), and  $\sigma_{max}$  is calculated for the time lapse between neighbouring pump pulses. In drawing curves, the pump power was assumed constant (17.5 kJ for the rod with the diameter of 4.5 cm, and 36.5 kJ for rods with the diameters of 6, 8.5, and 10 cm), whereas the pulse repetition rate  $f$  varied. In other words, Fig. 8 presents a parametrical functional dependence [ $\delta_R(f)$ ,  $\gamma(f)$ ,  $\sigma_{max}/\sigma_{lim}(f)$ ]. Calculations show that similar dependences for other pump energies limited above by the values of  $W_p$  from Table 1, are actually similar to those in Fig. 8, i.e., they are universal.

A combined analysis of the dependences of the energy stored in active elements versus the pump energy (Fig. 2) and dependences  $\sigma_{max}(\delta_R)$  and  $\delta_R(P_p)$  (Figs 8 and 7) allows one

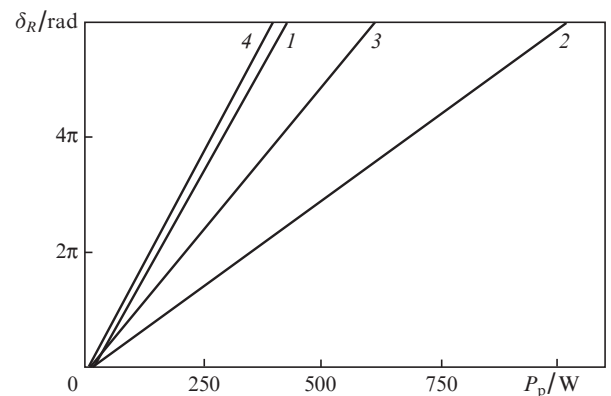


**Figure 7.** Difference of thermally induced phase increments for eigenwaves at the surface of an active element  $\delta_R$  vs. average pump power  $P_p$ . The diameters of the active elements are 4.5 (1), 6 (2), 8.5 (3), and 10 cm (4).

to determine attainable parameters of the repetitively pulsed operation regime for the laser amplifiers under study. Figure 9 shows attainable values of stored energy at various pump

pulse repetition rates. Each straight line in the figure corresponds to a constant phase difference  $\delta_R$  at the element edge, i.e., a constant ratio  $\sigma_{\max}/\sigma_{\text{lim}}$ .

The operation regimes with  $\delta_R = 4\pi$  rad (that is, according to Fig. 8,  $\sigma_{\max} = (0.2-0.25)\sigma_{\text{lim}}$ ) are, in our opinion, safe from the point of view of thermo-mechanical breakdown. This is confirmed by our experimental experience. In particular, in the experiments discussed in Section 3, the ratio  $\sigma_{\max}/\sigma_{\text{lim}}$  was 0.22 and the active element was not destroyed. The corresponding curves in Fig. 9 we will assume acceptable for determining an optimal relation between the pump pulse repetition rate and the energy stored in rods.

Plots in Figs 2, 7–9 give a possibility to calculate an arbitrary repetitively pulsed regime of operation for the amplifiers under study. Namely, at a prescribed pulse repetition rate  $f$  and maximal elastic stresses  $\sigma_{\max}$  at the rod edge one can find the pump energy  $W_p$  and corresponding stored energy  $W_{\text{st}}$  as well as thermally induced phase difference  $\delta_R$  for eigenwaves at the edge of an active element prior to the next pump pulse and the corresponding polarisation losses  $\gamma$ . In Table 2, the parameters of active elements under study are given, which provide their operation at the pulse repetition period of 1 or 2 min.

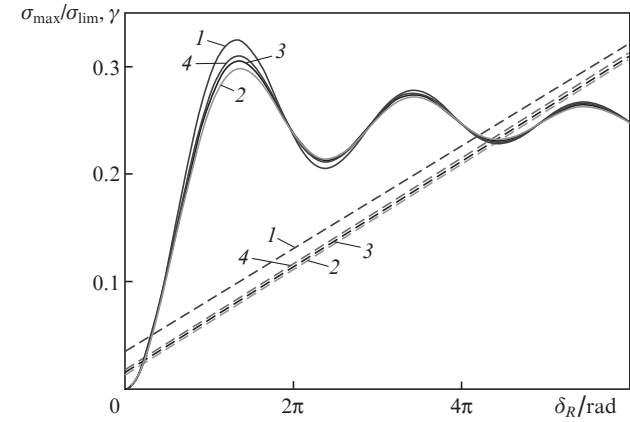


**Figure 8.** Integral coefficient of depolarisation  $\gamma$  (solid curves) and maximal elastic stresses  $\sigma_{\max}$  (dashed lines) vs. the phase difference of eigenwaves at the end of an active element  $\delta_R$ . The diameters of the active element are 4.5 (1), 6 (2), 8.5 (3), and 10 cm (4); the energy of pumping pulses is 17.5 kJ (1) and 36.5 kJ (2–4).

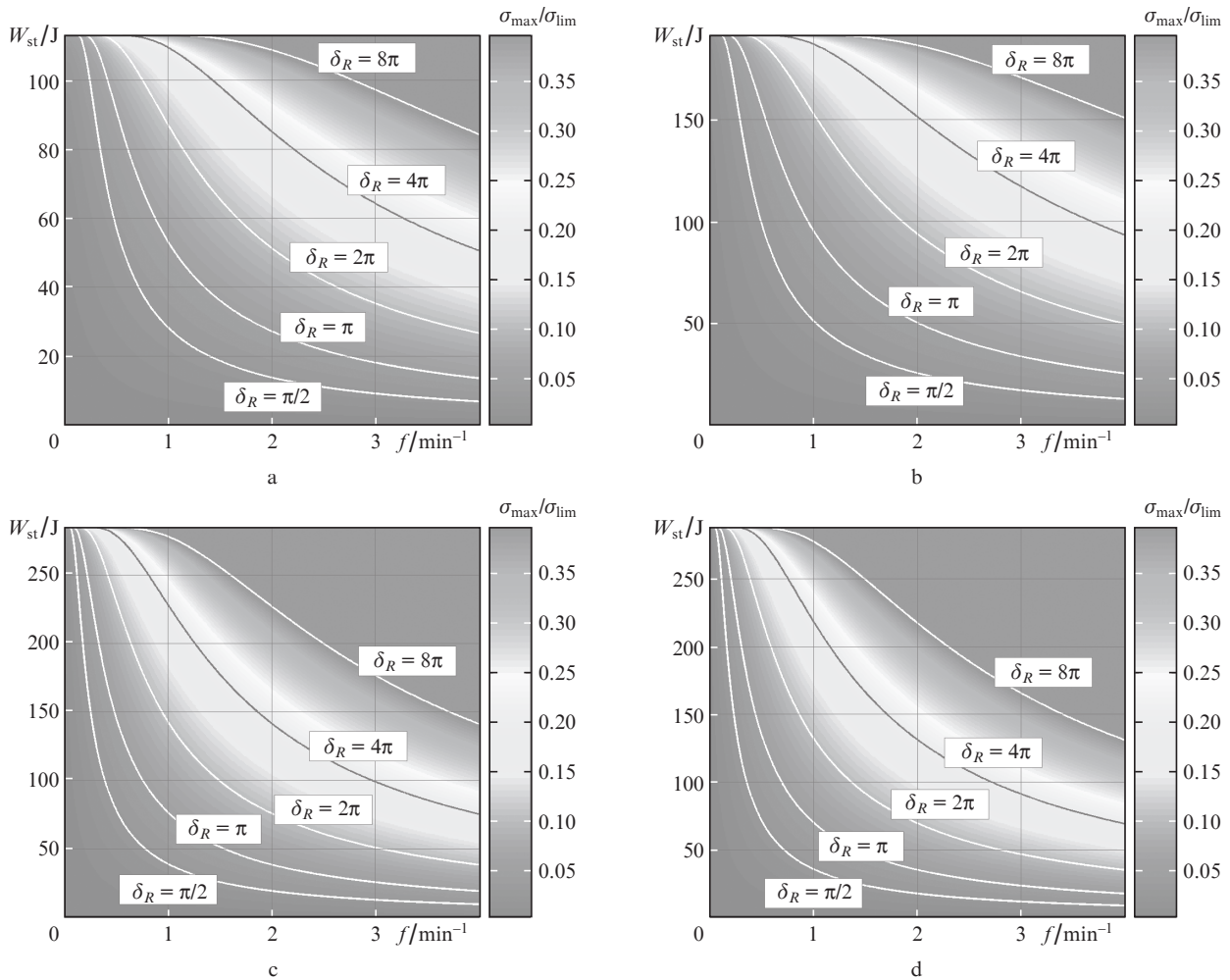


**Figure 9.** Constant phase difference curves  $\delta_R = \Delta\psi_\phi - \Delta\psi_r$  of the eigenwaves at the surface of active elements with the diameters of 4.5 (a), 6 (b), 8.5 (c), and 10 cm (d);  $\sigma_{\max}$  is a maximal elastic stress on the surface of the active element over the time lapse between pump pulses,  $\sigma_{\text{lim}} = 30$  MPa is the breakdown threshold for the KGSS-1621 glass.

Dependences in Fig. 9 show that at  $\delta_R = 4\pi$  rad, the maximal possible population inversion in the amplifiers with active element diameters of 6, 8.5, and 10 cm is safe if the pulse repetition period is at least 2–3 min. To transfer to the regime of 1 pulse  $\text{min}^{-1}$ , one should reduce the pump energy. This results in the stored energy reduced by 20%, which is noticeable because just large-aperture active elements are main accumulators of laser energy in high-power installations.

In a setup of PEARL type [3], an employment of active elements with an aperture of up to 10 cm is needed to prevent optical breakdown of rods by a laser pulse with the duration of 1 ns (the pulse energy is 300 J, the threshold of optical breakdown for glass at the pulse duration of 1 ns is  $10 \text{ J cm}^{-2}$ ). In the OPCPA scheme (Optical Parametrical Chirped Pulse Amplification), longer pump pulses cannot be used, because a parametrical amplifier cannot accumulate energy due to population inversion and the pump pulse should be comparable with the duration of an expanded femtosecond pulse ( $\sim 1$  ns). Similar limitations exist in subpicosecond neodymium glass lasers, in which the duration of an expanded pulse is also  $\sim 1$  ns.

**Table 2.** Parameters of investigated laser amplifiers operating at the pulse repetition rate of 1 and 2 min.

Rod diameter/ cm	$\delta_R/\text{rad}$		$\sigma_{\max}/\sigma_{\text{lim}}$		$W_p/\text{kJ}$		$W_{\text{st}}/\text{J}$	
	1 min	2 min	1 min	2 min	1 min	2 min	1 min	2 min
4.5	$4\pi$	$1.8\pi$	0.22	0.12	17.5	17.5	109	109
6	$3.5\pi$	$1.7\pi$	0.19	0.1	36.5	36.5	184	184
8.5	$4.1\pi$	$2.9\pi$	0.21	0.16	25	36.5	230	264
10	$4.2\pi$	$3.7\pi$	0.21	0.2	$16.5^*$	30	224	275

\*The operation regime is not employed in the scheme for flashlamp ignition.

An alternate concept of creating high-power setups is laser amplification of chirped pulses in a Ti:Sapphire crystal. Second harmonic of a neodymium laser may be used for pumping Ti:Sapphire crystals as well as for parametrical pumping of DKDP crystals; however, long pulses may ( $\sim 20$  ns) be employed in this case. At longer laser pulse durations the threshold breakdown intensity increases proportionally to the pulse duration in the one-half power. The threshold optical breakdown intensity of neodymium glass for such pulses is  $\sim 40 \text{ J cm}^{-2}$ ; hence, for generating pulses with the energy of several hundred joules one may employ active elements with an aperture less than 8.5 or 10 cm capable of operating at an increased pulse repetition rate. According to Figs 9a, b, and Table 2, active elements with the aperture of 4.5 or 6 cm operate safely (if  $\sigma_{\max}/\sigma_{\text{lim}}$  is 0.2 or less) at the repetition rate

1 pulse  $\text{min}^{-1}$  at the energy stored in population inversion close to a maximum admissible value.

However, the five-fold safety factor of neodymium glass itself is not sufficient for amplifier operation. A high-quality beam can only be obtained if strong polarisation and phase distortions are compensated. One known method of such compensation is employment of a  $90^\circ$  polarisation rotator placed between two similar amplifiers. In the following section, we present experimental results demonstrating the efficiency of such an approach.

## 5. Experimental study of depolarisation compensation in a laser for pumping Ti:Sapphire

Using the results given above we calculated a scheme for a high-power neodymium glass laser with the pulse energy of several hundred joules and pulse repetition rate of 1 pulse  $\text{min}^{-1}$ . Radiation of the laser converted to the second harmonic is used for pumping a Ti:Sapphire crystal. A schematic diagram of the power unit of the system is given in Fig. 10. It comprises four amplifiers on KGSS-1621 neodymium glass with the diameter of 4.5 cm (see Table 1). Radiation from a start unit is split by a polariser into two linearly polarised beams with equal energies. After two-pass amplification, radiation from both the channels is added and passes to a nonlinear crystal for frequency doubling (e–o–e synchronism). For efficient frequency doubling by e–o–e synchronism it suffices that the energies of an ordinary and extraordinary rays be equal and a phase difference between them be inessential. This provides frequency doubling of radiation from two non-phased channels.

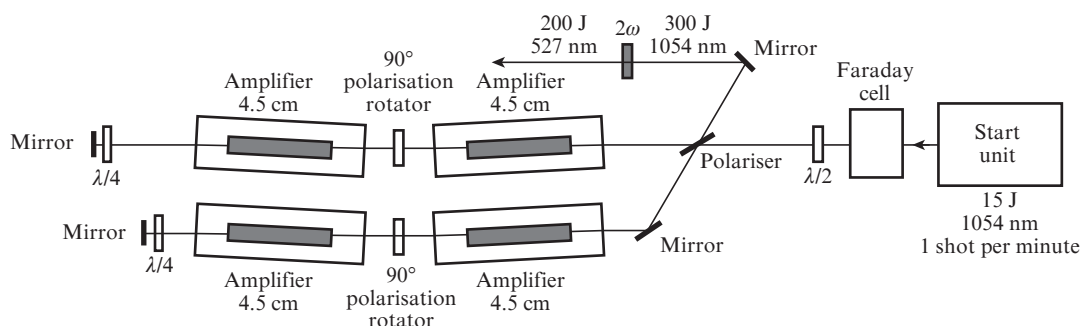
The intensity distribution at the amplifier input used for calculating laser output parameters is as follows

$$I_{\text{in}}(t, r) = I_0 \exp[-(2t/t_0)^2] \cos^2(\pi r^2/2R^2),$$

where  $t$  and  $r$  are temporal and radial coordinates, respectively,  $t_0 = 20$  ns,  $R = 2.25$  cm. The  $B$ -integral was calculated by the formula

$$B = 2\pi\gamma_{\text{NL}}\lambda^{-1} \max_{r,t} \left( \int_0^L I dz \right),$$

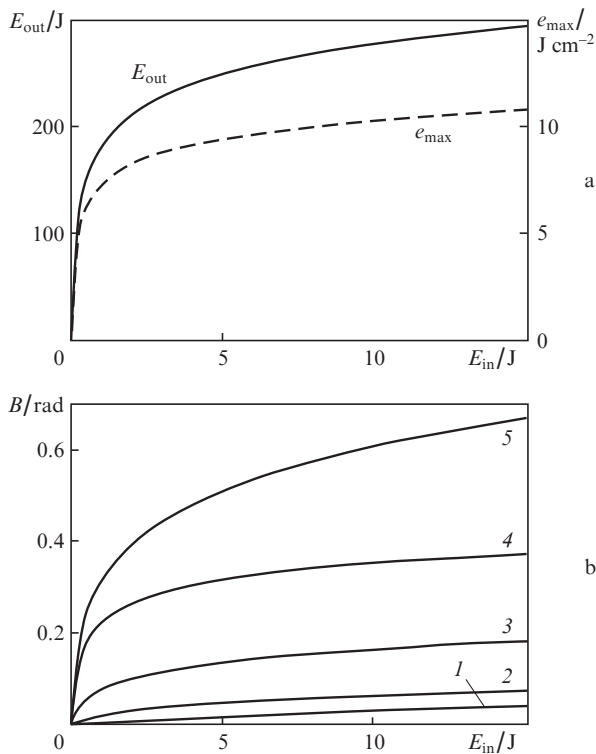
where  $L$  is the rod length,  $I$  is laser radiation intensity,  $\lambda$  is wavelength,  $\gamma_{\text{NL}}$  is the nonlinearity factor for neodymium glass (for a linear polarisation it was taken  $3.2 \times 10^{-7} \text{ cm}^2 \text{ GW}^{-1}$ ). The losses in the amplification scheme that were taken into



**Figure 10.** Schematic of a power unit of a laser pumping a Ti:Sapphire crystal.

**Table 3.** Losses in the amplifier scheme (Fig. 10) taken into account in calculations.

Schematic unit	Losses (%)
Polariser	10
Rod face	0.5
Rod body	5
90° polarisation rotator	0.5
Plate $\lambda/4$ (two passes) and a mirror	1

**Figure 11.** Laser output parameters vs. pulse energy of the start unit  $E_{in}$ : energy of the pulse  $E_{out}$  just in front of a frequency doubler and a maximal energy density  $e_{max}$  (a); increment of the  $B$ -integral (b) in an amplifier channel during the first passage through the first and second active elements with the diameters of 4.5 cm [curves (1) and (2), respectively], during the second passage through the second and first rods [curves (3) and (4), respectively] and the sum  $B$ -integral in a channel [curve (5)].

account in the calculations are given in Table 3. In Fig. 11, calculated output laser parameters are shown versus the pulse energy of the setup start unit

$$E_{in} = 2\pi \int_{-\infty}^{+\infty} dt \int_0^R I_{in}(r, t) r dr.$$

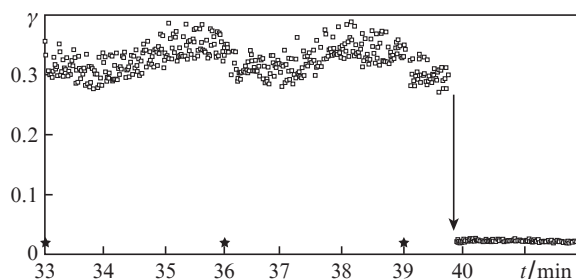
A solid curve in Fig. 11a presents the amplifier output energy  $E_{out}$  just before entering the frequency doubler, a dotted line in the figure describes a maximal energy density  $e_{max}$  in the beam. In Fig. 11b, increments of the  $B$ -integral are presented for each passage through the amplifier with the diameter of 4.5 cm [curves (1–4)] and the total  $B$ -integral for each of the amplifier channels [curve (5)].

Thus, if the start unit of the setup generates 20-ns pulses with the energy of 15 J, then the energy at the amplifier output will be 300 J in the first harmonic (Fig. 11a) or, at least, 200 J in the second harmonic (at the wavelength of 527 nm). A maximal expected radiation energy density is  $\sim 10.8 \text{ J cm}^{-2}$ , which

is below the optical breakdown threshold by a factor of 3 and more. The total  $B$ -integral in each power channel will be  $\sim 0.7$  rad, which is well below the threshold for developing a small-scale self-focusing instability.

In the calculations, we made allowance for overlapping of pulses of the first and second passes. The distances between the active elements and between the highly reflecting mirror and nearest amplifier (Fig. 10) were taken 60 and 20 cm, respectively. These values were chosen for more compact placement of the amplifiers on an optical table. Our experiments show that, despite a high ( $\sim 3000$ ) small-signal two-pass gain in channels, the role of spontaneous emission in the scheme considered is negligible. Note that if the distance from the highly reflecting mirror to a nearest amplifier is longer than 3 m, then the pulses of the first and second passes do not overlap. Calculations show that in this case the energy of the pulse passing to a crystal-doubler is  $\sim 320$  J at the start unit pulse energy of 15 J.

The setup is intended for operation in the regime of 1 pulse  $\text{min}^{-1}$ . Thermally induced birefringence is assumed to be compensated by a quartz 90° polarisation rotator placed between the active elements in each channel. A compensation possibility was demonstrated experimentally. We studied a thermally induced depolarisation of radiation in one of the channels of the laser comprising two double-pass active elements with the diameter of 4.5 cm (see Fig. 10). The pump pulse repetition period was 3 min. The energy of the pump pulses in each amplifier was 14.6 kJ. The value of depolarisation takes a stationary value  $\gamma \approx 30\%$  after 14 pump pulses without the 90° polarisation rotator. Then at the instant  $t = 39.8$  min, a 90° polarisation rotator was placed into the scheme, which resulted in an abrupt fall of  $\gamma$  (see Fig. 12).

**Figure 12.** Reduction of the integral coefficient of depolarisation in a scheme with two double-pass active elements with the diameters of 4.5 cm and a 90° polarisation rotator installed between them. Instants of pump pulses are marked with asterisks. The pump energy in each amplifier is  $W_p = 14.6$  kJ.

The experiment carried out demonstrates the reduction of the depolarisation factor from 0.35 to 0.02, which is close to the factor of cold depolarisation, by employing a 90° polarisation rotator. Along with data presented in Fig. 11a, this demonstrates advanced properties of the scheme for obtaining the output pulse energy of  $\sim 300$  J in first harmonic.

## 6. Conclusions

Thermally induced distortions of radiation in rod active elements with the diameter of 4.5 cm are experimentally studied. It is shown that at the pulse repetition rate of 1 pulse  $\text{min}^{-1}$  and the pumping providing the stored energy of above 100 J such an amplifier exhibits a five-fold safety factor with respect

to the thermo-mechanical breakdown threshold, which guarantees its safe operation.

It is shown that measurements of radiation thermally induced depolarisation in an active element can be used not only for controlling variations in beam polarisation, but also for diagnosing phase distortions of radiation and estimating the safety factor of the rod.

Based on the experimental data obtained we have analysed a repetitively pulsed operation regime for laser amplifiers with neodymium glass rods with the apertures of 4.5, 6, 8.5, and 10 cm. Universal dependences are obtained, which allow one not only to determine upper limits for the pulse repetition rate, but also to find a compromise between increasing the pulse repetition rate and enhancing the gain.

In particular, the results obtained show a possibility of creating a compact laser with a second harmonic pulse power of 200–250 J and the pulse repetition period of 1 min for pumping Ti:Sapphire crystals. The terminal stage of the laser is based on two pairs of amplifiers with the aperture of 4.5 cm. The designed gain and compensation of thermally induced depolarisation in a pair of such amplifiers have been demonstrated experimentally.

## References

1. Perry M.D., Pennington D., Stuart B.C., Tietbohl G., Britten J.A., Brown C., Herman S., Golick B., Kartz M., Miller J., Powell H.T., Vergino M., Yvanovsky V. *Opt. Lett.*, **24**, 160 (1999).
2. Aouama M., Yamakawa K., Akahane Y., Ma J., Inoue N., Ueda H., Kiriya H. *Opt. Lett.*, **28**, 1594 (2003).
3. Lozhkarev V.V., Freidman G.I., Ginzburg V.N., Katin E.V., Khazanov E.A., Kirsanov A.V., Luchinin G.A., Mal'shakov A.N., Martyanov M.A., Palashov O.V., Poteomkin A.K., Sergeev A.M., Shaykin A.A., Yakovlev I.V. *Laser Phys. Lett.*, **4**, 421 (2007).
4. Koechner W. *Solid State Laser Engineering* (New York: Springer, 2006).
5. Mezenov A.B., Soms L.N., Stepanov A.I. *Termooptika tverdotel'nykh lazerov* (Thermooptics of Solid-State Lasers) (Leningrad: Mashinostroenie, 1986).
6. Anan'ev Yu.A., Grishmanova N.I. *Zh. Prikl. Spektrosk.*, **12**, 668 (1970) [*J. Appl. Spectrosc.*, **12**, 503 (1970)].
7. Koechner W., Rice D.K. *IEEE J. Quantum Electron.*, **6**, 557 (1970).
8. Chun M.K., Bischoff J.T. *IEEE J. Quantum Electron.*, **7**, 200 (1971).
9. Mak A.A., Mit'kin V.M., Soms L.N. *Optiko-mekhanicheskaya promyshlennost'*, **9**, 65 (1971).
10. Vitrishchak I.B., Soms L.N., Tarasov A.A. *Zh. Tekh. Fiz.*, **44**, 1055 (1974).
11. Uppal J.S., Gupta P.D., Bhawalkar D.D. *J. Appl. Phys.*, **54**, 6615 (1983).
12. Gopi N., Nathan T.P.S., Sinha B.K. *Appl. Opt.*, **29**, 2259 (1990).
13. Kuz'min A.A., Luchinin G.A., Potyomkin A.K., Solov'yov A.A., Khazanov E.A., Shaikin A.A. *Kvantovaya Elektron.*, **39**, 895 (2009) [*Quantum Electron.*, **39**, 895 (2009)].
14. Bunkenberg J., Boles J., Brown D.C., Eastman J., Hoose J., Hopkins R., Iwan L., Jacobs S.D., Kelly J.H., Kumpan S., Letzring S., Lonobile D., Lund L.D., Mourou G., Refermat S., Seka W., Soures J.M., Walsh K. *IEEE J. Quantum Electron.*, **17**, 1620 (1981).
15. Kuzmin A.A., Khazanov E.A., Shaykin A.A. *Opt. Express*, **15**, 14223 (2011).
16. Avakyants L.I., Buzhinskii I.M., Koryagina E.I., Surkova V.F. *Kvantovaya Elektron.*, **5**, 725 (1078) [*Sov. J. Quantum Electron.*, **8**, 423 (1078)].
17. Potemkin A.K., Zhurin K.A., Kirsanov A.V., Kopelovich E.A., Kuznetsov M.V., Kuz'min A.A., Flat F.A., Khazanov E.A., Shaikin A.A. *Kvantovaya Elektron.*, **41**, 487 (2011) [*Quantum Electron.*, **41**, 487 (2011)].
18. Siegrist M.R. *Appl. Opt.*, **15**, 2167 (1976).